

# Journal of Materials Chemistry A

Accepted Manuscript



This is an *Accepted Manuscript*, which has been through the Royal Society of Chemistry peer review process and has been accepted for publication.

*Accepted Manuscripts* are published online shortly after acceptance, before technical editing, formatting and proof reading. Using this free service, authors can make their results available to the community, in citable form, before we publish the edited article. We will replace this *Accepted Manuscript* with the edited and formatted *Advance Article* as soon as it is available.

You can find more information about *Accepted Manuscripts* in the [Information for Authors](#).

Please note that technical editing may introduce minor changes to the text and/or graphics, which may alter content. The journal's standard [Terms & Conditions](#) and the [Ethical guidelines](#) still apply. In no event shall the Royal Society of Chemistry be held responsible for any errors or omissions in this *Accepted Manuscript* or any consequences arising from the use of any information it contains.

## Enhanced Photoelectrochemical Performance of CdSe Quantum Dots Sensitized SrTiO<sub>3</sub>

Gosipathala Sreedhar,<sup>a\*</sup> A. Sivanantham,<sup>a</sup> S. Venkateshwaran,<sup>b</sup> Subhendu K. Panda<sup>b\*</sup> and M.  
Eashwar<sup>c</sup>

## Abstract

We report the design and character of a novel CdSe quantum dot sensitized SrTiO<sub>3</sub> as photoanode for photoelectrochemical water splitting with strong absorption in the UV and visible light up to 607 nm and an enhanced photocatalytic water splitting activity. Our results demonstrate an increase of photo current density with a decrease of band gap of CdSe QDs for the sensitized SrTiO<sub>3</sub> electrodes. Combinations of CdSe QDs of different band gaps produce a current density of up to ~5 mA/cm<sup>2</sup> at 0 V and ~18 mA/cm<sup>2</sup> at 0.75 V vs. Ag/AgCl. In comparison to the bare SrTiO<sub>3</sub> electrode, a two-time increase in the current density is noted for the CdSe QDs sensitized SrTiO<sub>3</sub> electrodes at 0.75 V vs. Ag/AgCl. Our results demonstrate for the first time that the SrTiO<sub>3</sub> perovskite sensitized with tuned band gap CdSe QDs heterostructures as photoelectrocatalyst for enhanced solar water splitting.

**Keywords:** perovskites, quantum dots, photoelectrocatalysts, water splitting, energy conversion

## Introduction

Improvements in solar light harvesting using efficient energy conversion materials are quite essential to solve global energy problems. In this regard, photocatalytic water splitting reaction to produce hydrogen is one of the promising processes, owing to the benefit of hydrogen as an eco-friendly and renewable energy source.<sup>1,2</sup> Since the first photoelectrochemical cell (PEC) for solar water splitting reported in 1972 by Fujishima and Honda,<sup>3</sup> numerous research efforts have been made to develop efficient photocatalysts for hydrogen production. Mostly, noble metals (Pt, Rh) and semiconductor metal oxides (TiO<sub>2</sub>, ZnO, WO<sub>3</sub>, SnO<sub>2</sub>) were investigated as electro- and photo catalyst in the water electrolysis.<sup>4-7</sup> However, noble metals are expensive and the metal oxide semiconductors have a lower absorption of visible light and also the conduction band (CB) is not as negative as that required for H<sub>2</sub> evolution that limits the photoelectrochemical splitting of water. As the solar spectrum consists of almost 50% visible light (400< $\lambda$ <800 nm), to achieve higher photocatalytic water splitting efficiency, quantum dots (QDs) are emerging as promising candidates as they have comparatively higher absorption coefficients in visible light.<sup>8</sup> QD sensitized semiconductors have also been developed as photoelectrocatalyst materials in which narrow band gap QDs are linked either chemically or physically on to the surface of the wide band gap host semiconducting materials.<sup>9-12</sup> Among the reported QDs of metal chalcogenide photocatalysts, CdSe has been proven to be a good candidate for its excellent water splitting property due to its tunable band gap of 1.8 to 3.0 eV that matches well with the spectrum of sunlight, it has a high absorption cross-section and can move the conduction band edge of semiconductor to the more negative, so as to improve the possibilities to favour the H<sub>2</sub>O/H<sub>2</sub> redox reactions.<sup>13,14</sup> In this regard, several heterostructures have been developed using CdSe QDs such as CdSe/TiO<sub>2</sub>,<sup>15</sup> CdSe/CdS/ZnO,<sup>16</sup> CdSe/CdS/TiO<sub>2</sub>,<sup>17</sup> CdS/CdSe/ZnO,<sup>18</sup> CdSe/ZnS/ZnO,<sup>19</sup> CdS/CdSe/ZnO/TiO<sub>2</sub>,<sup>20</sup> and CdSe/SiNWs<sup>21</sup> emphasizing the role of band gap alignment in efficient water splitting.

In recent years, ternary perovskite structured strontium titanate ( $\text{SrTiO}_3$ , STO) is identified as one of the most suitable materials in energy conversion devices due to its unique electronic band structure and unidirectional charge transfer properties. The more negative conduction band (CB) edge of STO provides overall water splitting.<sup>22,23</sup> However, due to its wide band gap (3.4 eV), STO absorbs only the UV region of the solar spectrum (i.e.  $\sim 4\%$ ) resulting in low  $\text{H}_2$  gas evolution efficiency.<sup>24</sup> To enhance the visible light absorption, STO band gap is also tuned by doping various noble metals like Pt, Rh, Ru, Ir and transition metals like Cr and Mn, which extends the absorbance window to a certain extent in the visible range.<sup>25</sup> Alternatively, there are very few reports on heterostructures based STO photoanodes for solar water splitting. Townsend et al., reported that NiO-STO photoelectrodes generated photocurrent of  $10 \mu\text{A}/\text{cm}^2$  and  $28 \mu\text{mol H}_2 \text{ g}^{-1} \text{ h}^{-1}$  in KCl electrolyte.<sup>26</sup> The authors also proposed that the bulk STO activity found to be higher than the nano sized STO due to a quantum size effect. Wang et al. reported photocurrent density of  $0.5 \text{ mA}/\text{cm}^2$  using carbon QDs sensitized STO. The low currents produced were due to the limitation that carbon QDs sensitized STO absorbs solar light in the UV and IR regions only.<sup>27</sup> In this aspect, it would be interesting to investigate the photoelectrochemical water splitting behaviour of STO heterostructures utilizing low band gap semiconductor QDs that absorb in the visible region.

The present work describes the preparation of an efficient photoelectrode comprising of STO sensitized with CdSe quantum dots. The band gap tuned CdSe quantum dots absorb most of the visible light and transfer the photo-generated electrons to STO, which is involved in the water splitting mechanism. The tuned band gap CdSe QDs sensitized STO electrodes produced a photocurrent of  $1 \text{ mA}/\text{cm}^2$  at 0 V (vs. Ag/AgCl). Due to the improved photocurrent density and the synergistic effect of various sized CdSe QDs, our photoanodes showed substantially enhanced water splitting efficiency. To our knowledge, CdSe QDs sensitized STO heterostructure as a photoelectrode for solar water splitting has not been explored.

## Experimental

Synthesis of SrTiO<sub>3</sub>: SrTiO<sub>3</sub> were synthesized via hydrothermal route. Ten mmol of each sarcosine hydrochloride (99%, Alfa Aesar) and lithium bis (trifluoromethyl sulfonyl) imide (TFSI) (98+%, Alfa Aesar) were dissolved separately in 10 mL of de-ionised water, and mixed together under stirring at room temperature for 30 min. A clear, transparent lithiated sarcosine solution was obtained. Further, equimolar (0.65 M) of Sr(OH)<sub>2</sub> · 6H<sub>2</sub>O and TiCl<sub>4</sub> were separately dissolved in 10 mL of ionic solution and mixed together. Then, 10 M NaOH solution was added to the above mixture and continuously stirred for 30 min. The above solution was transferred into a 50 ml Teflon-lined stainless steel autoclave, kept at 170 °C for 16 h and then cooled to room temperature. The obtained product was washed several times using de-ionised water by centrifugation and finally dried at 80 °C in air for 5 h. The obtained product was calcinated at 800 °C for 24 h.

Synthesis of CdSe QDs: Various sized CdSe QDs were synthesized by following our previous reported work.<sup>28</sup> Cadmium oxide (CdO, 99%), 1-hexadecylamine (HDA, 99%), tri-n-octylphosphine (TOP, 90%), tri-noctylphosphineoxide (TOPO, 99%), oleic acid and selenium powder (Se, 99.99%) were purchased from sigma Aldrich. In a typical synthesis using three-neck flask, 0.2 mmol of CdO and 0.5 g of oleic acid (OA) were heated to 180 °C until the mixture became clear and then cooled down to room temperature. Three ml of HDA and 6 ml of TOPO were added to the mixture and degassed again at 100 °C for 15 minutes. The mixture was then heated to 280 °C under vigorous stirring and 1 ml of 1 M TOPSe was swiftly injected. The temperature was lowered to 260 °C for the nanocrystal growth. To get the desired green, yellow and red fluorescent QDs, the reaction solution was suddenly cooled to room temperature at 1 min, 2 min and 4 min respectively by putting a water bath below the flask. Then the QDs were washed with toluene/methanol solvent by centrifugation at 3000 rpm and then stored in toluene. In order to exchange the OA with MPA, 1 mL of the toluene solution containing 50 mg of OA capped CdSe

were mixed with 1 mL of acetone and 1 mL of MPA. The resulting precipitate containing MPA capped CdSe QDs was dissolved and stored in de-ionized water.

Sensitization of CdSe QDs on SrTiO<sub>3</sub>: Ten mg of MPA capped CdSe in de-ionised water was mixed with 20 mg of SrTiO<sub>3</sub> powder (1:2 weight ratios) and continuously stirred for 4 h. The linking mechanism is shown as scheme S1 (See Supporting Information) which is supported by FTIR data (Figure S1, See Supporting Information). For the mixed QDs system, 1:1 wt. ratio i.e. 5 mg from each of the two types of QDs were mixed together and then added to 20 mg of SrTiO<sub>3</sub> powder so as to maintain the 1:2 weight ratio with SrTiO<sub>3</sub>. The final product was washed using ethanol and collected as a CdSe QDs sensitized SrTiO<sub>3</sub> (CdSe QDs/STO). All photo electrodes were prepared on indium tin oxide coated glass films using simple squeegee method for photoelectrochemical studies.<sup>29</sup>

Structural and Optical Characterization: The chemical bonding between QD and STO through MPA was studied by using Infra-red spectroscopy (Brucker-Tensor27, 400-2000 cm<sup>-1</sup>). The phase and crystallinity of SrTiO<sub>3</sub> and CdSe QDs were analysed using X-ray diffraction (Bruker-Advanced D8, 2θ range from 20 - 70°). Optical characterizations were carried out using UV-Vis Spectroscopy (Speccord 200 Plus, 200-800 nm). Morphological analysis was done using Transition Electron Microscopy (TEM, Technai G<sup>2</sup> 20). The performance of photoelectrochemical water splitting was recorded using a typical three electrode potentiostat system (Bio-Logic, Model: VMP3 and EC-Lab software, version 10.31) with a Pt counter electrode, Ag/AgCl reference electrode and photocatalyst material coated ITO plate as the working electrode (with 1 cm<sup>2</sup> exposure area). The exposure area of working electrode was illuminated with a solar-simulated light source (power intensity of 100 mW/cm<sup>2</sup> from 300 W Xe lamp passing through an AM 1.5G filter Model-SS80AA). Linear sweep voltammograms were obtained at the scan rate of 10 mV/s. The electrolyte used was an aqueous solution of 1 M Na<sub>2</sub>S (pH=13), which is a sacrificial electrolyte that inhibits the photo corrosion of CdSe QDs. The electrolyte was bubbled with nitrogen stream before the commencement of

photoelectrochemical studies. Incident photoelectric conversion efficiency was measured using IPCE measurement kit, where a monochromator (300 W Xe lamp) was used to obtain the monochromatic light. The IPCE was defined as the following equation:

$$\text{IPCE (\%)} = \{(1240 * I_{\text{ph}}) / (\lambda \text{ (nm)} * J_{\text{light}})\} * 100$$

Where,  $I_{\text{ph}}$  is photocurrent densities ( $\text{mA}/\text{cm}^2$ ),  $\lambda$  is wavelength (nm) of incident light and  $J_{\text{light}}$  is incident light power density ( $\text{mW}/\text{cm}^2$ ). The amount of hydrogen evolved was determined using a gas chromatograph (CP-4900 Micro-GC). Argon gas was purged through the reaction cell for 30 min before reaction to remove air. The experiments were conducted in 1 M  $\text{Na}_2\text{S}$  electrolyte with zero bias voltage.

## Results and Discussion

We synthesized both STO and CdSe QDs, and explored their optical and photocatalytic characteristics. Fig. 1a is a digital image of the CdSe QDs fluorescing under UV illumination and exhibiting green, yellow and red colouration. The three different colours essentially resulted from particle size differences in the CdSe QDs. Fig. 1b presents the absorption spectra for the above CdSe QDs. Particle sizes for the CdSe QDs were determined as 2.2, 3.4 and 4.2 nm, from the absorbance peaks noticed at 503, 560 and 607 nm, respectively. The relationship between the maximum in the  $1S_e-1S_h$  transition position ( $\lambda_{\text{Abs,max}}$ ) and the CdSe nanoparticle size and the extinction coefficient is taken from the work of Peng et al.<sup>30</sup> The band gaps were calculated from the first excitonic peak (Fig. 1b) and found to be 2.5, 2.2 and 2.0 eV for G-, Y-, and R-CdSe QDs respectively. The photoluminescence spectra for the CdSe QDs (Fig. 1c) indicate the highly luminescent QDs originating from band edge emissions.

It is important for a photo anode to have maximum light absorption ranging from blue to red region of the solar spectrum for efficient water splitting. In this regard, CdSe QDs such as green (G), yellow (Y) and red (R), either individually or in combination (GR and YR), were sensitized on STO and their absorption behaviour studied. Fig. 2a,b depicts absorption spectra for bare STO and

CdSe QDs-sensitized STO in the UV and visible regions, respectively. The spectrum for bare STO reveals absorption only in the UV region (358 nm) corresponding to a band gap of 3.46 eV (see supporting information, Fig. S3). With CdSe sensitization, absorption peaks are noted in both UV as well as respective visible regions. Further, as revealed in Fig. 2b, the combination GR-STO shows high absorption in green (530 nm) as well as red (610 nm) regions. Similarly, YR-STO shows absorbance in both yellow (570 nm) and red (610 nm) regions.

The XRD spectra for bare R-CdSe, STO and CdSe-sensitized STO are shown in Fig. 3a,b and c respectively. The representative spectrum of R-CdSe QDs exhibits three major peaks corresponding to the (111), (220) and (311) planes and confirming the cubic phase (JCPDS # 19-0191). The broadened peaks for all the planes indicate the nanostructure of the CdSe QDs. The crystallite size for the red QD was calculated from the (111) plane by using Debye-Scherrer equation is  $\sim 4.7$  nm corresponding to the d-spacing value of  $3.53 \text{ \AA}$ . The diffraction peaks for STO (3b) are identical to the cubic phase (JCPDS # 79-0176), while the crystallite size calculated from the (110) plane of STO is  $\sim 53.3$  nm corresponding to the d-spacing value of  $2.75 \text{ \AA}$ . The XRD spectrum in Fig. 3c for CdSe sensitized STO shows the major peaks corresponding to both STO and CdSe QDs. The peaks corresponding to CdSe QD and STO are marked as \* and # respectively. As the STO peak intensities are very high so a zoomed spectra is given (Fig. 3c), which clearly demonstrates the presence of broadened CdSe peaks along with the STO peaks.

HRTEM images for bare CdSe (Fig. 4a-c), are clearly indicate that the CdSe QDs are highly crystalline in nature showing well defined lattice fringes. The particle size estimated are 2.2, 3.5 and 4.3 nm for G,Y and R-CdSe QDs, respectively, which corroborated with the particle size calculation from UV absorbance data. The TEM images of STO (Fig. 4d) shows that the STO is highly crystalline and cubic shaped morphology. The size found between 70 and 110 nm, with an average of  $85 \pm 15$  nm. The porosity of the particles is internal rather than surface active sites, which is explained in our earlier work.<sup>31</sup> The internal porosity formed due to the in-sufficient diffusion of Sr

ions in to the already formed  $\text{TiO}_2$  crystallites. The TEM images for R-CdSe QDs sensitized STO are shown in Fig 4e & f. From the figure, the R-CdSe QDs attachment on the surface of STO is evidenced by the increase in the surface roughness. The SAED pattern for bare R-CdSe in Fig. 4g shows bright circles corresponds to (111), (220) and (311) planes indicating polycrystalline nature of the R-CdSe QDs. Fig. 4h shows the SAED pattern of pristine STO conforming single crystalline nature. CdSe-sensitized STO (Fig. 4i) shows rings for the CdSe as well as dots for the STO, thus confirming the presence of both materials. Surface morphological features (FESEM images) of electrodes are also supported the presence of QDs on STO surface (Fig. S2, See Supporting Information).

When the CdSe-STO photoanode is irradiated by UV-visible light, both CdSe and STO are excited and the generated electrons in CdSe are transferred to the CB of STO, then further transferred to the Pt foil (counter electrode) where protons are reduced and  $\text{H}_2$  generation occurs. Simultaneously, the holes move to the photoanode/electrolyte interface and are collected by the hole scavengers ( $\text{S}^{2-}$ ). Photoelectrochemical measurements were carried out with bare QDs, bare STO and CdSe-STO, and the effect of sensitization was examined towards photo response in water splitting. The prepared photoanodes (G-STO, Y-STO, R-STO, GR-STO and YR-STO) were used as working electrodes in an aqueous solution of 1 M  $\text{Na}_2\text{S}$ . Linear sweep voltammograms (I-V curves) were recorded on various photoanodes under dark and illuminated conditions with a constant light intensity of  $100 \text{ mW/cm}^2$ . Fig. 5a illustrates the action spectra for bare QDs and the maximum photocurrent density of  $\sim 3.9 \text{ mA/cm}^2$  was obtained for red QDs at 0.75 V vs. Ag/AgCl. Fig. 5b shows the set of LSVs recorded for the bare STO and CdSe QDs sensitized STO photoanodes. Bare STO showed current densities of  $0.5 \text{ mA/cm}^2$  and  $0.8 \text{ mA/cm}^2$  under dark and illuminated conditions respectively at 0 V vs. Ag/AgCl, pointing to a photo current density of  $0.3 \text{ mA/cm}^2$ . More significantly, sensitization with CdSe QDs (various band gaps) resulted in substantially enhanced photo current density as compared to bare STO photoanodes. The maximum photo current density recorded in this work was  $\sim 1 \text{ mA/cm}^2$  at 0 V vs. Ag/AgCl, for the sample YR-STO.

This is about three times higher than that for the bare STO sample. According to Townsend et al.,<sup>26</sup> the bulk STO particles are observed to be beneficial for water splitting application hence our synthesized  $85 \pm 15$  nm STO particles are also shown higher photoelectrochemical water splitting performance. Further, the photocurrent of CdSe QDs sensitized STO is substantially enhanced due to the increase in the visible light absorption range. In this present study, the generated photo currents were considerably higher than those already reported in the literature for the STO based photoelectrodes for water splitting.<sup>26,27</sup> Fig. 5c extends the LSV data recorded for the bare STO and various band gap CdSe QDs sensitized STO photoanodes up to 0.75 V vs. Ag/AgCl ( $\sim 1.7$  V vs. RHE). The maximum current density of  $\sim 18$  mA/cm<sup>2</sup> was obtained from YR-STO photoanode, nearly two times higher than that for bare STO under illumination.

The effectiveness of CdSe QDs as a co-catalyst with STO in photoelectrochemical water splitting was assessed by IPCE measurements as a function of wavelength (Fig. 5d). The IPCE spectra of STO and QDs-STO are in good agreement with the corresponding UV-Vis absorption spectra (Fig. 2). The single band gap QDs sensitized STO photoanodes (G-STO (15.2%), Y-STO (8.3%) and R-STO (20.3%)) exhibited a significantly higher IPCE at different wavelengths (510 nm, 540 nm and 590 nm respectively) than that of bare STO (8.8%) at 360 nm. This indicates that the IPCE response of QDs-STO reflects the synergy arising from the excited interaction between CdSe and STO. Interestingly, when two different band gap QDs sensitized STO photoanode (GR-STO (26.2%) and YR-STO (30.5%)) was used, the IPCE values as high as can be achieved in the wavelengths range of 540-620 nm and 580-640 nm respectively. This result indicates that number of excited electrons can increase than those in single band gap CdSe QDs and effectively injected into STO and thus become collected by the electrode.

From Fig. 5 it can be clearly observed that the photo current density follows a trend as shown below:

$$\text{Bare STO} < \text{G-STO} < \text{Y-STO} < \text{R-STO} < \text{GR-STO} < \text{YR-STO}$$

where the photo current increased with decreasing band gap of the CdSe, from 2.5 eV to 2.0 eV, in other words from green to red. This may be due to the reason that a decrease in the band gap of the QDs also results in a lowering of the distance between the CB of the CdSe QDs and STO. This can facilitate higher electron transfer rate from the CdSe QDs to STO and consequently enhanced efficiency. This demonstrates that the absorption of solar light can be maximized by tuning the band gap of the CdSe QDs and also by mixing QDs of various band gaps. Our results also clearly exemplify the unique advantage in employing varied band gaps of CdSe QDs sensitization on perovskite STO photoanodes for enhanced photo currents and enhanced efficiency in water splitting.

Fig. 6 shows the reaction time dependent photoelectrocatalytic H<sub>2</sub> evolution plots by different samples in 1 M sacrificial electrolyte (Na<sub>2</sub>S) under solar light irradiation with applied potential of 0.75 V vs. Ag/AgCl.<sup>32,33</sup> All photoanodes exhibited the steady performance for the period of 4 h experiment (See Supporting Information for i-t curves, Fig S4). In comparison to the bare STO (41 μmol.g<sup>-1</sup>) all co-catalyst (QDs) sensitized STO photoanodes exhibit higher H<sub>2</sub> evolution due to the visible light absorption of co-catalyst. Among them, more than 100 μmol.g<sup>-1</sup> of H<sub>2</sub> was evolved from mixed QDs sensitized STO (YR-STO – 120.9 μmol.g<sup>-1</sup> and GR-STO – 112.3 μmol.g<sup>-1</sup>) in a prolonged experiment (4 h). The single QDs sensitized STO also having the enhanced H<sub>2</sub> evolution, which was about more than 50 μmol.g<sup>-1</sup> (G-STO – 57.3 μmol.g<sup>-1</sup>, Y-STO – 78.7 μmol.g<sup>-1</sup> and R-STO – 89.9 μmol.g<sup>-1</sup>).

## Conclusions

We have reported a CdSe QDs sensitized STO photoelectrocatalyst material for an enhanced water splitting performance. Higher photo current density of ~1 mA/cm<sup>2</sup> was drawn from CdSe/STO photoelectrocatalyst in a sacrificial 1 M Na<sub>2</sub>S aqueous solution at 0 V vs. Ag/AgCl. The highest current density of 18 mA/cm<sup>2</sup> was obtained at 0.75 V vs. Ag/AgCl for mixed band gap QDs sensitized STO anodes. This work has demonstrated the advantages of tuned band gap CdSe QDs

sensitization on STO towards water splitting. This protocol may be further optimized to achieve higher IPCE. We expect that our new approach for the fabrication of CdSe/STO will be applicable to the synthesis of various novel heterostructures using various QDs for high efficiency perovskite solar energy conversion and hydrogen generation devices.

### Supporting Information

Electronic Supplementary Information (ESI) available: The CdSe QDs sensitization scheme, FTIR, FESEM, Tauc Plot, i-t curves and Table is present in supporting information. See DOI: 10.1039/c000000x/

### Acknowledgements

Dr. G. Sreedhar would like to acknowledge the Electro-Inorganic Division, CSIR- CECRI, for allowing the use of solar simulator. Dr. Panda would like to thank Department of Science and Technology, Government of India, for the financial support (Project no: SB/FT/CS-048/2012). Dr. Eashwar would like to thank CSIR-CECRI for financial support (MULTIFUN, Project no: CSC0101F).

### Notes and References

<sup>a</sup>Electrolyro Metallurgy Division, CSIR-Central Electrochemical Research Institute, Karaikudi, Tamil Nadu- 630006, India. E-Mail: gsreedhar@cecri.res.in.

<sup>b</sup>EMFT Division, CSIR-Central Electrochemical Research Institute, Karaikudi, Tamil Nadu- 630006, India. E-Mail: skpanda@cecri.res.in.

<sup>c</sup>Corrosion Testing Centre, CSIR-Central Electrochemical Research Institute, Mandapam Camp, Tamil Nadu- 623519, India.

1. X. Li, J. Yu, J. Low, Y. Fang, J. Xiao and X. Chen, *J. Mater. Chem. A*, 2015, **3**, 2485.
2. M. G. Walter, E. L. Warren, J. R. McKone, S. W. Boettcher, Q. Mi, E. A. Santori and N. S. Lewis, *Chem. Rev.*, 2010, **110**, 6446.
3. A. Fujishima and K. Honda, *Nature*, 1972, **238**, 37.
4. F. E. Osterloh, *Chem. Soc. Rev.*, 2013, **42**, 2294.
5. S. Hernández, D. Hidalgo, A. Sacco, A. Chiodoni, A. Lamberti, V. Cauda, E. Tresso and G. Saracco, *Phys. Chem. Chem. Phys.*, 2015, **17**, 7775.
6. J. Su, L. Guo, N. Bao and C. A. Grimes, *Nano Lett.*, 2011, **11**, 1928,
7. R. Saito, Y. Miseki and K. Sayama, *Chem. Commun.*, 2012, **48**, 3833.
8. W.W. Yu, L. Qu, W. Guo and X. Peng, *Chem. Mater.*, 2003, 15, 2854–2860.
9. I. Robel, M. Kuno and P. V. Kamat, *J. Am. Chem. Soc.*, 2007, **129**, 4136.
10. S. Chaguetmi, F. Mammeri, S. Nowak, P. Decorse, H. Lecoq, M. Gaceur, J. B. Naceur, S. Achour, R. Chtourou and S. Ammar, *RSC Adv.*, 2013, **3**, 2572;
11. Y. Tak, S. J. Hong, J. S. Lee and K. Yong, *Crystal Growth & Design*, 2009, **9**, 2627;
12. F. Aldeek, C. Mustin, L. Balan, G. Medjahdi, T. R. Carmes, P. Arnoux and R. Schneider, *Eur. J. Inorg. Chem.*, 2011, 794.
13. F. A. Frame, E. C. Carroll, D. S. Larsen, M. Sarahan, N. D. Browning and F. E. Osterloh, *Chem Comm.*, 2008, 2206.
14. A. Kongkanand, K. Tvrdy, K. Takechi, M. Kuno and P.V. Kamat, *J. Am. Chem. Soc.*, 2008, **130**, 4007.
15. L. Liu, J. Hensel, R. C. Fitzmorris, Y. Li, and J. Z. Zhang, *J. Phys. Chem. Lett.*, 2010, **1**, 155.
16. M. Seol, H. Kim, W. Kim and K. Yong, *Electrochem. Commun.*, 2010, **12**, 1416.
17. H. Wang, W. Zhu, B. Chong and K. Qin, *Int. J. Hydrogen Energy*, 2014, **39**, 90.
18. G. Wang, X. Yang, F. Qian, J. Z. Zhang and Y. Li, *Nano Lett.*, 2010, **10**, 1088.
19. J. Huang, S. Liu, L. Kuang, Y. Zhao, T. Jiang, S. Liu and X. Xu, *J. Environ. Sci.*, 2013, **25**, 2487.

20. Z. Ali, I. Shakir and D. J. Kang, *J. Mater. Chem. A*, 2014, **2**, 6474.
21. R. R. Devarapalli, C. K. Kamaja and M. V. Shelke, *J. Mater. Chem. A*, 2014, **2**, 13352
22. Z. Jiao, T. Chen, J. Xiong, T. Wang, G. Lu, J. Ye and Y. Bi, *Scientific Reports*, 2013, **3**, 2720.
23. M. G. Walter, E. L. Warren, J. R. McKone, S. W. Boettcher, Q. Mi, E. A. Santori and N. S. Lewis, *Chem. Rev.*, 2010, **110**, 6446.
24. X. Chen and C. Burda, *J. Am. Chem. Soc.*, 2008, **130**, 5018; M. Takizawa, K. Maekawa, H. Wadati, T. Yoshida, A. Fujimori, H. Kumigashira and M. Oshima, *Phys. Rev. B*, 2009, **79**, 113103.
25. H. C. Chen, C. W. Huang, J. C. S. Wu and S. T. Lin, *J. Phys. Chem. C*, 2012, **116**, 7897; P. Reunchan, N. Umezawa, S. Ouyanga and J. Ye, *Phys. Chem. Chem. Phys.*, 2012, **14**, 1876; A. K. Wahab, T. Odedairo, J. Labis, M. Hedhili, A. Delavar and H. Idriss, *Appl. Petrochem. Res.*, 2013, **3**, 83; H. Yu, S. Ouyang, S. Yan, Z. Li, T. Yu and Z. Zou, *J. Mater. Chem.*, 2011, **21**, 11347; F. E. Osterloh, *Chem. Mater.*, 2008, **20**, 35; H. Kato, Y. Sasaki, N. Shirakura and A. Kudo, *J. Mater. Chem. A*, 2013, **1**, 12327.
26. T. K. Townsend, N. D. Browning, and F. E. Osterloh, *ACS Nano*, 2012, **6**, 7420.
27. F. Wang, Y. Liu, Z. Ma, H. Li, Z. Kang and M. Shen, *New J. Chem.*, 2013, **37**, 290.
28. L. Etgar, J. Park, C. Barolo, V. Lesnyak, S. K. Panda, P. Quagliotto, S. G. Hickey, M. K. Nazeeruddin, A. Eychmueller, G. Viscardi and M. Gratzel, *RSC Advances*, 2012, **2**, 2748; S. K. Panda, S. G. Hickey, C. Waurisch and A. Eychmueller, *J. Mater. Chem.*, 2011, **21**, 11550.
29. K. Iwashina and A. Kudo, *J. Am. Chem. Soc.*, 2011, **133**, 13272;
30. W. W. Yu, L. Qu, W. Guo and X. Peng, *Chem. Mater.*, 2003, **15**, 2854.
31. G. Sreedhar, A. Sivanantham, T. Baskaran, R. Rajapandian, S. Vengatesan, L. J. Berchmans, and S.G. Babu, *Mater. Lett.* 2014, **133**, 127.
32. Y. Myung, D. M. Jang, T. K. Sung, Y. J. Sohn, G. B. Jung, Y. J. Cho, H. S. Kim and J. Park, *ACS Nano*, 2010, **4**, 3789.
33. A. Kudo and M. Sekizawa, *Chem. Comm.*, 2000, 1371.

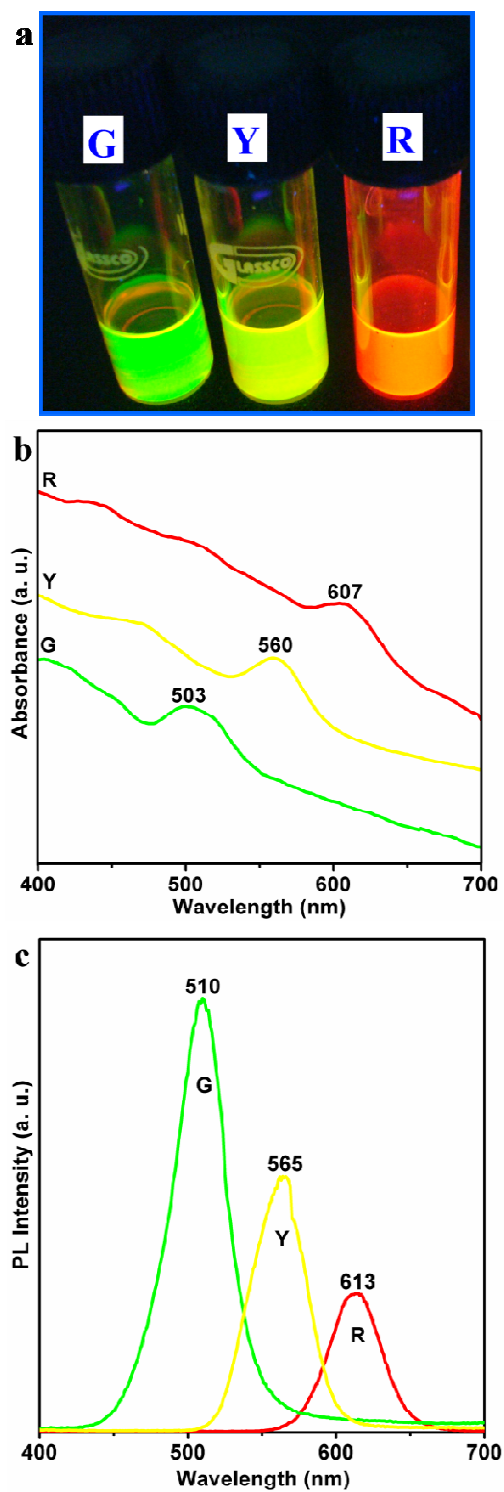


**Fig. 1** (a) Fluorescence image (b) UV- Vis absorbance spectra (c) PL spectra of, Green (G), Yellow (Y) and Red (R) CdSe QDs photo electrodes.

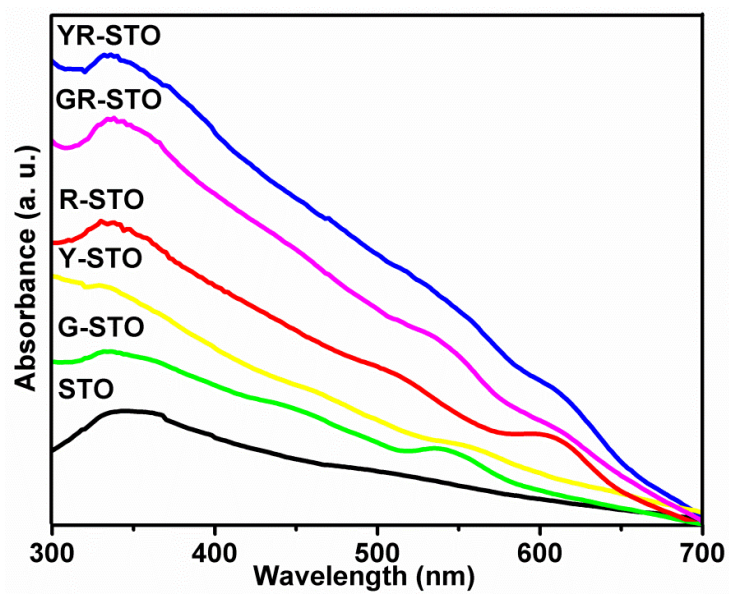


**Fig. 2** UV-Vis absorption spectra of CdSe QDs-STO photo electrodes.

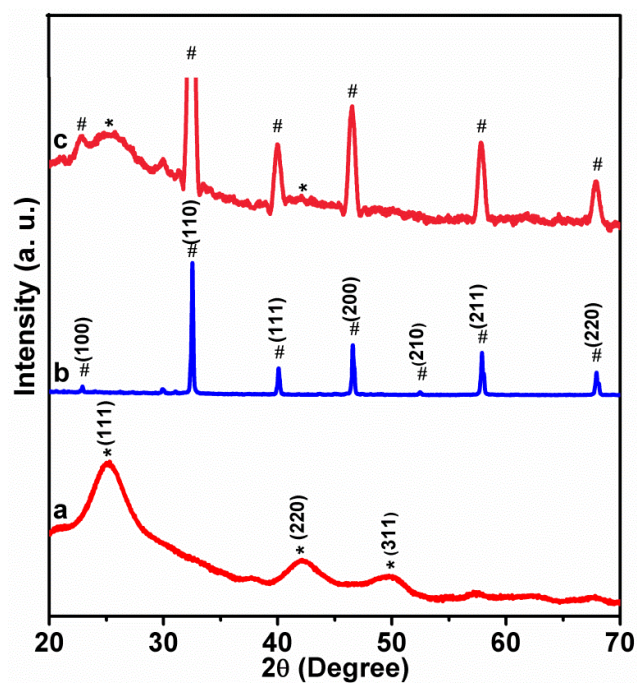


**Fig. 3** XRD patterns of (a) R- CdSe QDs (b) STO (c) R-CdSe QDs-STO photo electrodes.

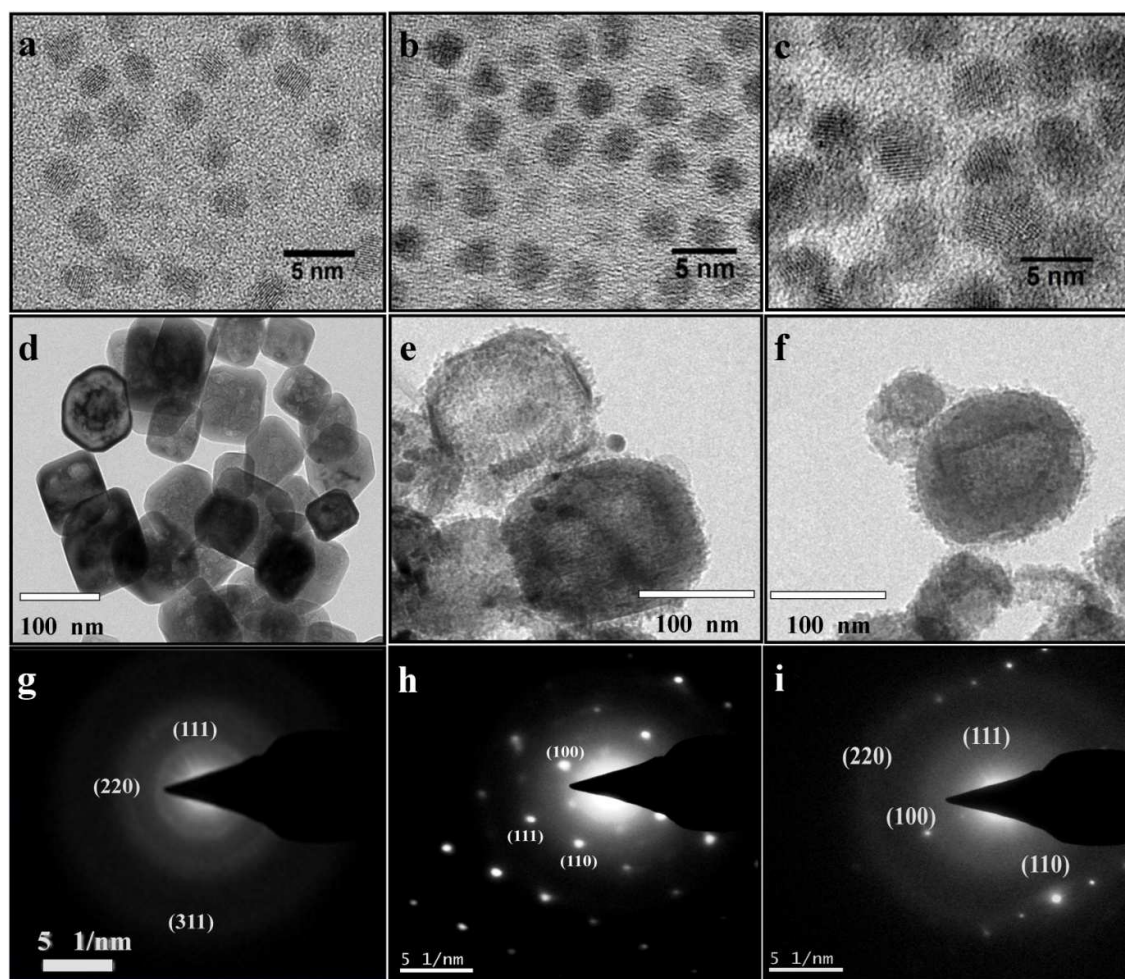


**Fig. 4** HRTEM image of CdSe QDs (a-c) and TEM images of STO (d) and R-CdSe-STO (e&f) and SAED patterns for R-CdSe (g), STO (h) and R-CdSe-STO (i) compounds.

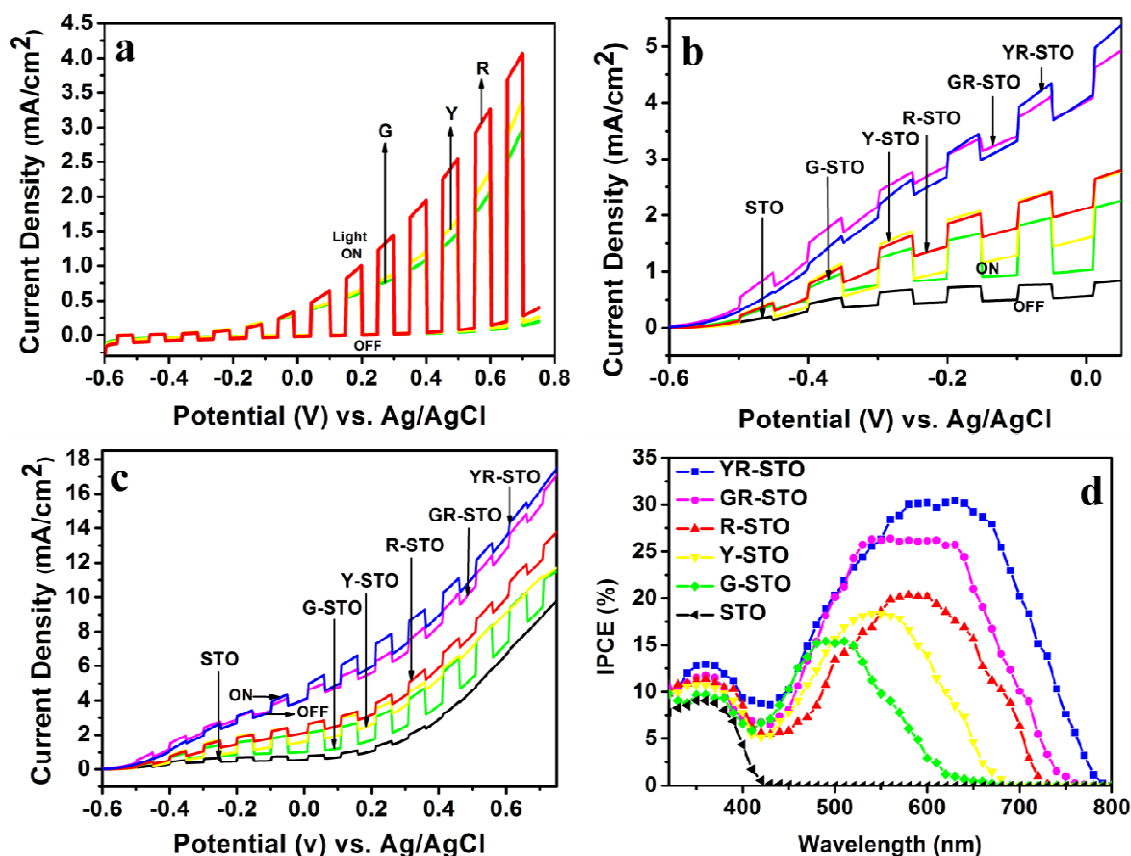


**Fig. 5** Linear sweep voltammograms (LSV) of the photo electrodes (a) Bare QDs (b) QDs-STO, potential from -0.6 to 0 V(vs. Ag/AgCl) (c) QDs-STO, potential from -0.6 to 0.75 V under dark and light (simulated AM 1.5 G illumination of 100 mW/cm<sup>2</sup>) in 1 M Na<sub>2</sub>S solution at a scan rate of 10 mV/s and (d) IPCE spectra of bare STO and QDs sensitized STO photo electrodes using solar simulator with band gap filters, collected at the incident wavelength range from 320 to 800 nm in 1 M Na<sub>2</sub>S electrolyte with zero bias voltage.

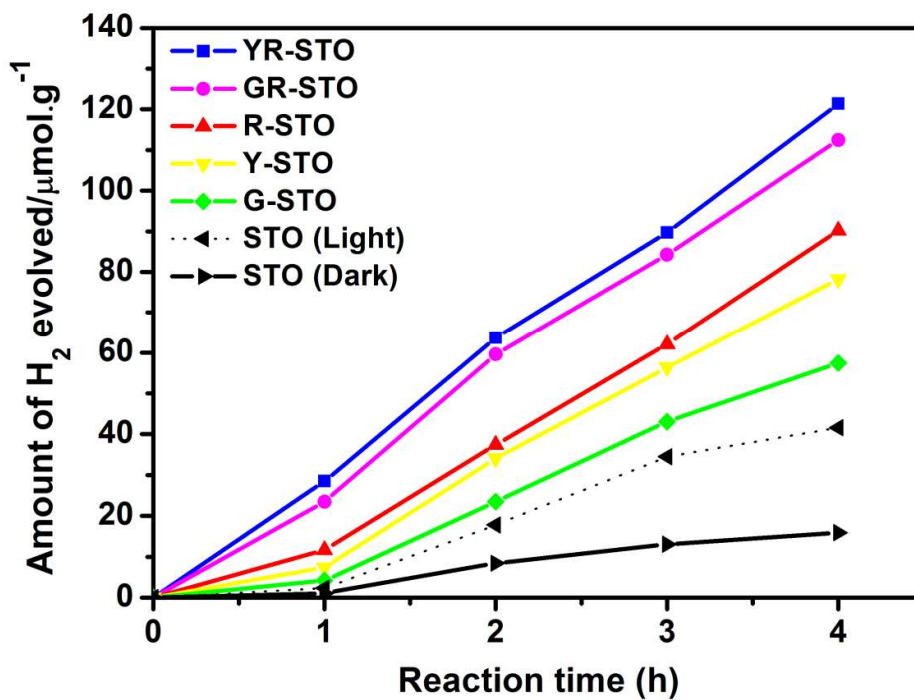


**Fig. 6** Amount of hydrogen evolved from the bare STO and CdSe QDs-STO photo electrodes in 1M Na<sub>2</sub>S solution at 0.75 V vs. Ag/AgCl.

## Table of Content

Efficient water splitting performance of novel CdSe/SrTiO<sub>3</sub> photoanodes is studied. CdSe quantum dots with various band gaps are sensitized on SrTiO<sub>3</sub>. Enhanced photo current density is achieved up to ~1 mA/cm<sup>2</sup> at 0 V vs. Ag/AgCl.

